Composites Part A 118 (2019) 250–258

Contents lists available at ScienceDirect

Composites Part A

journal homepage: www.elsevier.com/locate/compositesa

Highly mechanical nanostructured aramid-composites with gradient structures

Yanghao Ou, Meiyan Lin, Lingfeng Su, Xiao Feng, Ming Wang, Jun Li, Detao Liu*, Haisong Qi*

State Key Laboratory of Pulp and Paper Engineering, South China University of Technology, Guangzhou 510640, China
Guangdong Engineering Research Center for Green Fine Chemicals, South China University of Technology, Guangzhou 510640, China

ARTICLE INFO

Keywords:
Aramid nano-composites
Reinforcement
Surface modification
Mechanical properties

ABSTRACT

In this work, we reported a gradient structure that can significantly improve the mechanical strength of aramid paper by depositing a layer of nano-aramid fibers (ANFs) on both sides. The introduction of Dimethyl Diallyl Ammonium Chloride (DMDAAC) in the fabrication of nanostructured aramid-composites dramatically promotes the dewatering efficiency of the aramid nanofibers slurry, and also accelerates the formation of gradient structural of the composites. The gradient deposition of ANFs in the porous aramid paper matrix yields the highly pilotaxitic textures and stiff structures of the aramid composite paper. The results indicated that the tensile strength, specific strength, and fracture energy increased respectively 36.7 times, 14.1 times and 78.0 times from the original aramid paper. The method reported in this work gives a good case for designing the structure composites with low density and high strength in aerospace and car manufacturing applications.

1. Introduction

In recent years, aramid fiber with high molecular orientation and crystallinity has become a research hotspot due to its high specific strength, specific modulus, excellent heat resistance and dielectric performance [1–4]. Aramid paper made from aramid chopped fibers (ACFs) and aramid pulp fibers (APFs) was fabricated by the typical papermaking process. The obtained aramid paper has a variety of unique structures and properties, such as excellent chemical stability, low density, fairly good flame retardancy and thermal stability, high electrical insulation, and radiation resistance [5]. These features of aramid paper lead to the important applications of such environmental protection, energy and chemical industry [6], sensors [7], aerospace, electric products [8–10], rail transit [11], defense and military industry.

However, due to the smooth surface and extremely low surface chemical activity of aramid fibers [12], it is difficult to disperse uniformly them in aqueous medium, making it difficult to obtain a paper with good uniformity and strength. The mechanical strength of aramid paper is mainly attributed to the random physical bridging between the fibers and their own rigidity [5,13]. Because of its less fiber interweaving, the weak part of aramid paper firstly breaking under the stress, leading to the decrease of overall strength. More recently, many research efforts have been devoted to improving the surface activity of aramid fibers by chemical etching and grafting [12,14–17], plasma surface modification [18–21], high-energy radiation [22], ultrasonic radiation [23], ultraviolet radiation [24] and so on. They can effectively improve the surface activity and surface roughness of aramid fibers, and thus the dispersity of aramid fibers in water. However, its special features including the extremely long aspect ratio results the difficulty in achieving the uniform structures and outstanding properties comparable to the ordinary plant fiber paper. Therefore, there is thereby an urgent need but it is still a significant challenge to have a substantial improvement of aramid paper's mechanical strength.

According to the principle of fracture mechanics, the destruction of materials normally has two stages: one is the existence of cracks inside the material, and the other is that such cracks can propagate through the material until it breaks [25]. The reinforcement for the weaker part of the paper by using reinforcing materials is an effective pathway to fabricate the highly mechanical composite paper. It optimizes the whole structure of the paper to be evenly balanced, which can greatly reduce the chance of the first break from the weak part.

Interestingly, Kotov's group had discovered that aramid fibers was completely split into aramid nanofibers (ANFs) in dimethyl sulfoxide (DMSO) with the presence of some potassium hydroxide (KOH)[26]. The ANFs have diameters in the range of 5–30 nm and lengths in the range of 5–10 μm. The surficial formation of carboxylic acid, carbonyl, and hydroxyl groups onto ANFs, while retaining the stiff physical

* Corresponding authors.
E-mail addresses: dtliu@scut.edu.cn (D. Liu), qihs@scut.edu.cn (H. Qi).

https://doi.org/10.1016/j.compositesa.2019.01.003
Received 19 August 2018; Received in revised form 14 December 2018; Accepted 3 January 2019
Available online 05 January 2019
1359-835X/

properties and also the basically chemical composition compared to the pristine aramid fibers, indicates the possible potential in material design [26].

Since the ANFs were reported, there were many excellent reviews in the literature dealing with the concepts of ANFs, which significantly enhance the mechanical properties of the substrate. For instance, Yu et al. [27]. used ANFs to reinforce the PVA film and the obtained PVA/ANFs membrane shows a significant growth on tensile strength and toughness. Lin et al. [28]. added a certain amount of ANFs to the epoxy resin, which effectively changed the failure mode of the pure epoxy resin, improved the fracture resistance, and also enhanced the strength, stiffness, and toughness. In addition, ANFS can be embedded in nanocomposites as a new nanoscale component that can produce composite membranes with record ultimate strength and stiffness. Zhu et al. [29]. obtained MWCNTs/ANFs hybrid membranes by vacuum filtration, with tensile strength and Young's modulus being as high as 383 MPa and 35 GPa, respectively. Se at al. [30]. added a certain amount of ANFs in the preparation of graphene flexible capacitors, which achieved a great increase in strength. Taking into account the fact that the thermal properties of aramid nanofibers have not changed much compared with ACFs [26]. Consequently, ANFs can be considered as a perfect nanoreinforcement material that can effectively enhance the mechanical strength of aramid paper.

In this work, we firstly modified the aramid fiber with a coupling agent to increase the surface activity to maximize the formation of the original aramid paper (Fig. 1a). The structures of the N-(2-aminoethyl)-3-aminopropyltrimethoxysilane (KH-792) modified ACFs was investigated by scanning electron microscopy (SEM) and X-ray photoelectron spectroscopy (XPS) respectively (Fig. 2). Then a layer of ANFs was deposited on both sides of the aramid paper by vacuum filtration (Fig. 1c). According to DLOVE theory [31], the flocculation can be induced by electrostatic and long-range van der Waals force effect. Hence, we added a certain amount of positively charged Dimethyl Diallyl Ammonium Chloride (DMDAAC) to the ANFs solution to hasten the filtration process. Finally, the ANFs-reinforced paper can be fabricated by the hot-pressing process. Compared to that of the original aramid paper, the tensile strength, specific strength, and fracture energy of the ANFs-reinforced paper were increased 36.7 times, 14.1 times, and 78.0 times.

2. Materials and methods

2.1. Materials

Para-aramid chopped fibers (ACFs) and Para-aramid pulp fibers (APFs) with an average length between 5 and 6 mm were purchased from DuPont, Polyoxyethylene (PEO) (Mw = 3,000,000–4,000,000) were all supplied by Shanghai Maclean Biochemical Technology Co., Ltd. Coupling agents N-(2-aminoethyl)-3-aminopropyltrimethoxysilane (KH-792) provided by Jiangsu Chenguang Coupling Agent Co., Ltd. KOH and Dimethyl sulfoxide (DMSO) and Dimethyl Diallyl Ammonium Chloride (DMDAAC) were purchased from Shanghai Lingfeng Chemical Reagent Co., Ltd. Acetone was supplied by Tianjin Fuyu Fine Chemical Co., Ltd.

2.2. Surface modification of ACFs and APFs

Firstly, the ACFs and APFs were soaked with acetone and ultra-sonicated for 4 h with a power of 100 W for the purpose of swelling the fiber and removing impurities from the fiber surface. For a typical surface modification, ACFs and APFs were treated by coupling agent KH792 at a concentration of 20% (with 8% water and 72% ethanol) for

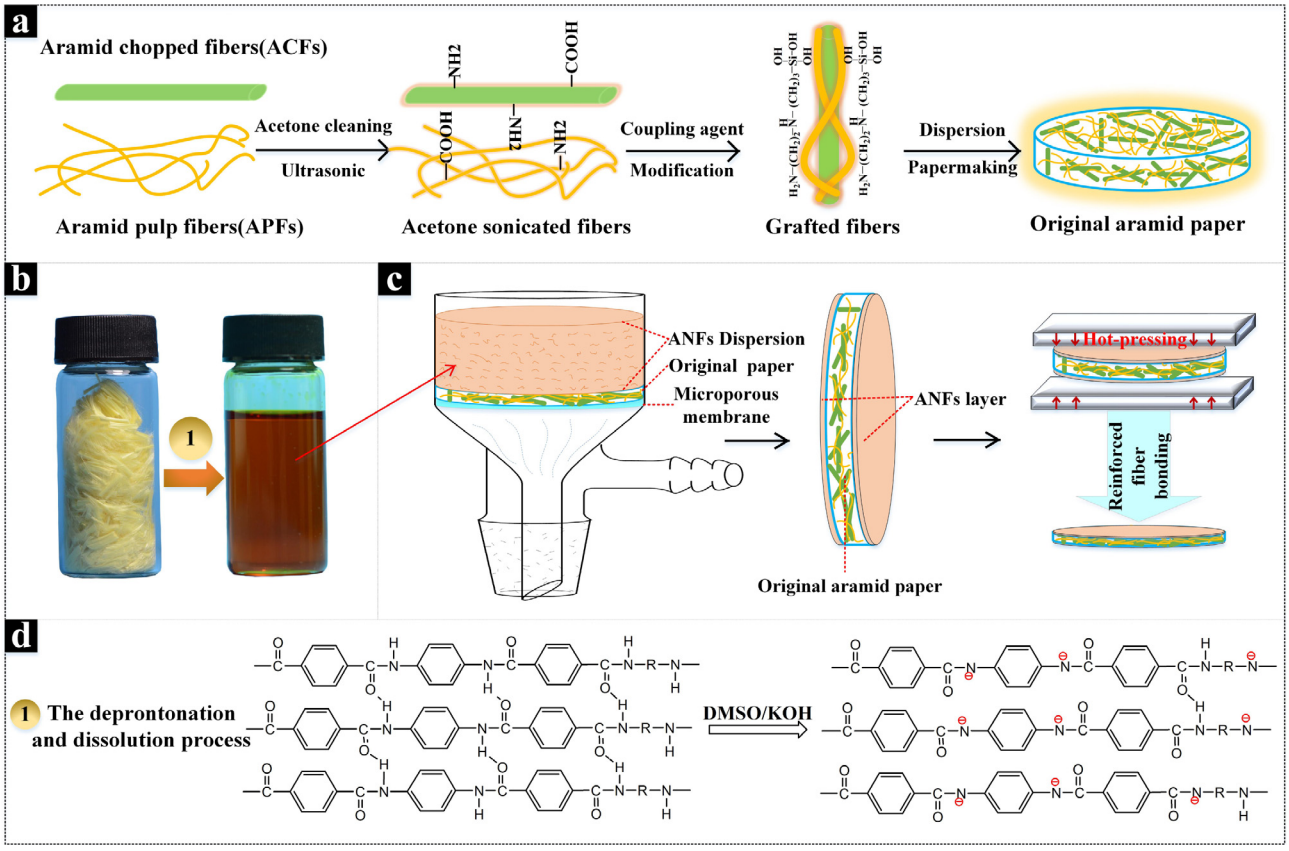

Fig. 1. (a) Schematic illustration of the aramid fiber modification process and the simple manufacturing process of original aramid paper. (b) Digital photo of ACFs and ANFs dispersions. (c) Schematic illustration of the original aramid paper reinforcement process. (d) The principle of preparing ANFs in DMSO solution. (For interpretation of the references to colour in this figure legend, the reader is referred to the web version of this article.)

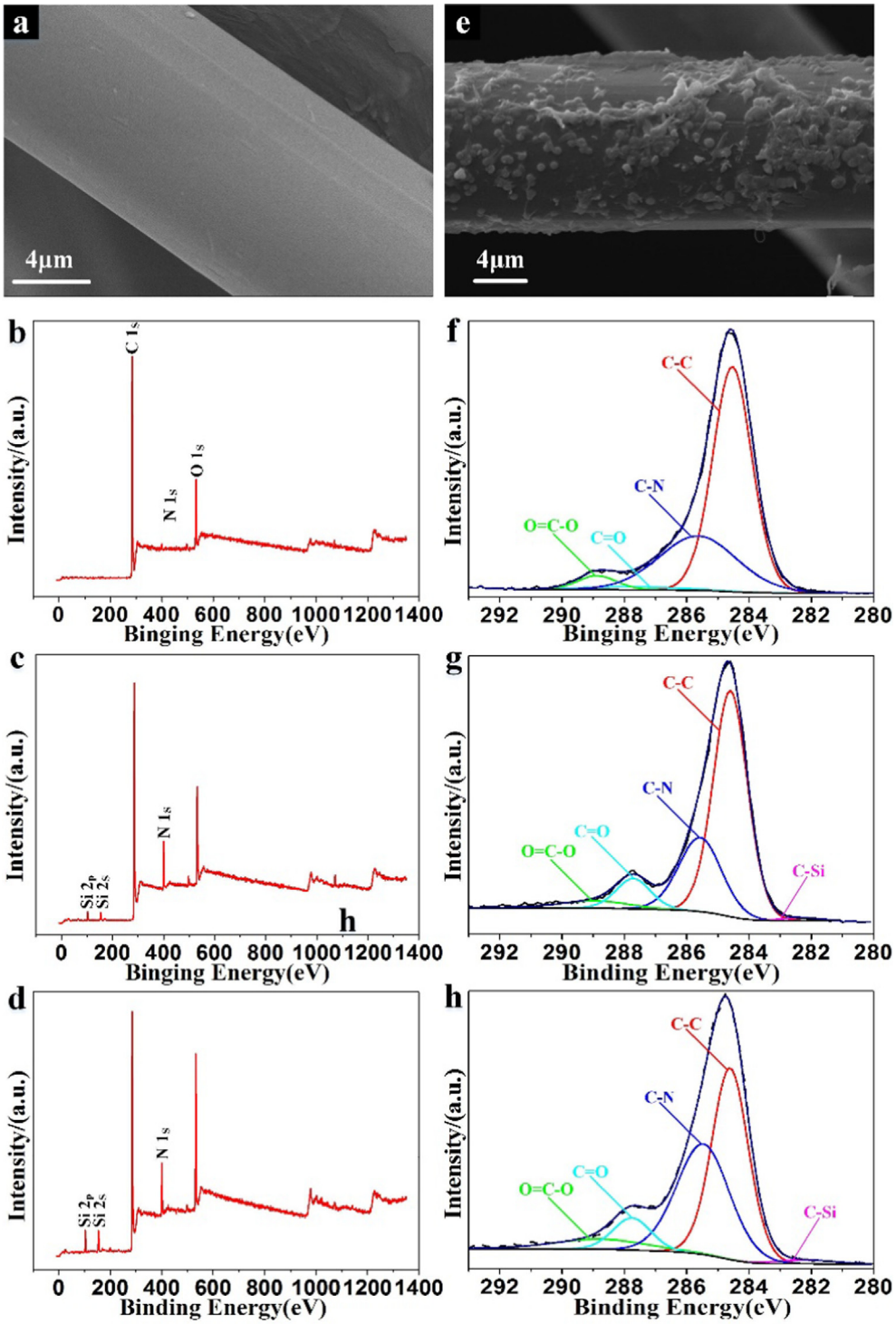

Fig. 2. SEM image (a) of untreated ACFs, (e) KH-792 modified ACFs. XPS wide-scan (b,c,d) and C 1 s core-level spectra (f,g,h) of untreated ACFs (b, f), acetone ultrasonicated ACFs(c, g), KH-792 modified ACFs(d, h). (For interpretation of the references to colour in this figure legend, the reader is referred to the web version of this article.)

4 h under 50 °C.

2.3. Preparation of aramid paper

Aramid paper composites were prepared by a hand sheet former (MESSMER 255) with a quantitative weighing of 80 g/m^2. The preparation process is depending on the following procedures. Firstly, the modified ACFs and APFs were fully mixed in a mass ratio of 4:6. Then the fibers were separated into single fibers in water by pulp disintegrator (L&W 991509, Sweden). Subsequently, 0.5 wt% PEO was added to the fiber suspension used as a dispersant, and then the fiber suspension was continuously defibered with a pulp disintegrator, the number of rotations was 30,000 r, and the rotation speed was 6000 rpm. Finally, the fiber suspension was all poured into the hand sheet former and dehydrated into the paper at one time.

2.4. Preparation of ANFs/DMSO dispersion

ANFs/DMSO dispersion was prepared by splitting the ACFs in DMSO with the aid of KOH as previously reported by Kotov's group [26]. The ACFs were soaked in acetone (99%) and ultra-sonicated for 4 h to wash the aramid fibers. After ultrasonic treatment, the ACFs were rinsed with deionized water and placed in a vacuum oven at 80° C for 24 h. Then, the treated ACFs(1 g) and KOH (1.5 g) were added into 500 mL DMSO. After magnetic stirring with a speed of 1500–2500 rpm for 7 days at room temperature. Finally get dark red ANFs/DMSO dispersion (2.0 mg/mL).

2.5. Fabrication of nanostructured aramid-composites

ANFs-reinforced aramid paper were prepared by a simple Filtration process (Fig. 1c). First, 5 mL ANFs/DMSO dispersion was diluted in 20 mL DMSO and stirred evenly, then add 15 mL DMDAAC solution (60 wt%) to the diluent and stir it evenly. At this point, the ANFs starts to flocculate due to electrostatic adsorption, and the color of the solution gradually fades (Fig. 4d). The ANFs/DMSO/DMDAAC mixture was vacuum filtered on a nylon filter membrane (47 mm diameter, 0.2 μm pore size). As we can see in Fig. 1, we put the original aramid paper on top of the nylon filter membrane, the aramid nanofibers are uniformly deposited on the paper by vacuum suction. Then, we also deposited ANFs on the other side of the paper with the same operation. The ANFs-reinforced paper was rinsed with water and carefully peeled from the nylon membrane and placed between PTFE membrane and dried at 80 °C in vacuum for 24 h. The reinforced paper was placed between two glass slides with 4 clips clamped to prevent bubble formation during the thermal reduction process. Finally, we pressed the aramid paper with a flat plate vulcanizer (BoLon Precision Testing Instrument Co., Ltd.) for 5 min, set the hot-pressing temperature to 220 °C and the pressure to 10 MPa (Fig. 1c).

2.6. Materials characterization

The structure of the ACFs and aramid paper was studied with a scanning electron microscope (SEM). JEM-100CXII at an accelerating voltage of 10 kV. Prior to the examination, the surface of the specimen was coated with a thin layer of gold, ~20 nm. Surface groups of aramid fibers were characterized by X-ray photoelectron spectroscopy (XPS) (Thermo scientific, America). The morphologies of ANFS were observed by transmission electron microscopy (TEM) (JEOL1400F) and AFM (Bruker Instruments, Germany), One drop of solution (0.1 mg mL^{-1}) was placed on the surface of a holey copper grid coated with carbon (TEM test) and clean wafers (AFM test) and the solvent was evaporated before characterization. The thickness was determined using a Thickness Tester (L&W, Sweden). The ILSS of samples was measured using a MONITOR/INTERNAL BOND (TMI model 80-01). The mechanical strength of samples was measured using a universal tensile tester (Instron5565, Instron instruments Inc. USA) with the stretching velocity of 5 mm/min. To prevent the sample from slipping during the test, we wrap the two ends of the sample with ordinary plant fiber paper and put them into the fixture together and tighten the screws as much as possible. Samples were first cut to 20.0 mm × 10.0 mm and placed in a constant temperature and humidity chamber at (50 ± 1) % relative humidity (RH) and (23 ± 1) °C for 24 h to ensure the stabilization of their water content before characterization. The thermogravimetric analyzer (TA Q500, USA) was utilized to analyze the thermal properties of ACFs and ANFs and reinforced paper. The test temperature range was 20 ~ 700 °C, and the heating rate was 10 °C min^{-1} with an air purge at a flow rate of 20 mL min^{-1}. The quality of each sample is controlled between 4 and 8 mg during the test.

3. Results and discussion

3.1. Surface characterizations of the coupling agent-modified ACFs

Firstly, the ACFs and APFs were ultra-sonicated with acetone for the purpose of removing impurities from the fiber surface and swelling the fiber to expose more active groups such as amino groups and amide groups on the surface [32,33]. For a potential surface modification, ACFs were treated by coupling agent KH-792. After the hydrolysis of KH-792. As shown in the below function, the $–Si(OCH_3)_3$ group is hydrolyzed to form a strong hydrophilic $-Si(OH)_3$, which is beneficial to the dispersion of aramid fibers in water. At the same time, the other part $-(CH_2)_3NH(CH_2)_2NH_2$ can graft to −COOH groups on the surface of aramid fibers through $-NH_2$ and −NH− groups (Fig. 1a).

$$NH_2(CH)_2NH(CH_2)_3Si(OCH_3)_3 + 3H_2O \rightarrow NH_2(CH)_2NH(CH_2)_3Si(OH)_3 + 3CH_3OH$$

The XPS was used to determine the surface composition of the aramid fiber. Fig. 2 shows the XPS wide scan of untreated fibers (Fig. 2b), acetone ultra-sonicated fibers (Fig. 2c), and KH-792 grafted fibers (Fig. 2d), respectively. The results of elemental content change are presented in Table 1. After the aramid fiber being ultrasonically treated with acetone, the contents of N and O on the fiber surface were increased, while the content of C was decreased obviously. The O/C ratio was increased from 16.90% to 20.93% and the N/C ratio was increased from 3.07% to 12.07%. It indicates an increase of surface active groups and surface energy for aramid fibers. Si element appears in the XPS spectrum of the original aramid fiber, which may be caused by the oil on the surface of the aramid fiber or the impurities adhering on the fiber during the XPS test. As for the Si element on the acetone ultra-sonicated fiber, it is due to the impact and erosion of the ultrasonic wave on the glass container [23], which causes the Si element to fall off and adhere to the surface of the aramid fiber. In order to investigate the chemical interaction during the acetone ultrasonic treatment, the deconvolution analysis of the C1s peak was performed and the results were presented in Fig. 2 and Table 2. For untreated aramid fibers, there are four peaks indicating C−C group (284.6 eV), C−N/C−O group (285.7 eV), C = O group (287.8 eV), and O═C−O group (288.9 eV) respectively. After acetone ultrasonic treatment, the ratio of oxygen-containing groups gradually increases from 36.57% to 37.27%, while the ratio for C–C group decreases from 63.43% to 61.84% (Table 2). In particular, the increase of C═O group from 2.25% to 8.36% indicates that the concentration of exposed −COOH groups on the fiber surface increase, which is beneficial to the subsequent grafting reaction with KH-792. As shown in Table 1, the surface elemental composition of fibers modified by KH-792 undergoes further changes compared to untreated fibers. The C element content sharply decreased

Table 1
Elements changes on the surface of untreated aramid fibers and treated fibers.

Samples	Chemical composition (%)				Atomic ratio (%)		
	C	O	N	Si	O/C	N/C	(O + N)/C
Untreated	82.73	13.98	2.54	0.76	16.90	3.07	19.97
Acetone sonicated	73.01	15.28	8.81	2.90	20.93	12.07	33.00
KH-792 modified	66.32	18.02	9.16	6.50	27.17	13.81	40.98

Table 2
Contents of functional groups on the surface of untreated fibers and treated fibers.

Samples	Concentrations of correlative functional groups (%)				
	C—C	C—N/C—O	O═C—O	C═O	C—Si
Untreated	63.43	30.38	3.94	2.25	0
Acetone sonicated	61.84	25.07	3.84	8.36	0.89
KH-792 modified	46.07	38.30	6.16	7.98	1.49

from 82.73% to 66.32%, while the Si element content is 6.50%, 8.55 times higher than the original fiber of 0.76%. At the same time, the O/C ratio and N/C ratio further increased to 27.17% and 13.81%, respectively. The C1s core-level spectrum of the KH-792 modified fiber could be curve-fitted with five peak components (Fig. 2h), including a new C-Si peak (282.2 eV) compared to the untreated aramid fibers (Fig. 2f). The content of this C-Si peak is 1.49%. Compared with the significant decrease of C—C group (284.6 eV), in addition, the contents of C-N/C-O group (285.5 eV), O═C—O (288.8 eV) group, and C═O (287.8 eV) group have also increased significantly (Table 2). This substantial increase of the oxygen group contents on the fiber side further demonstrates the successful modification of aramid fiber surface with KH-792, which will facilitate the dispersion of aramid fibers in water and the formation of paper.

The surface morphology of aramid fibers were investigated by SEM. Compared to the smooth surface of the untreated aramid fiber (Fig. 2a), the surface of the modified fiber becomes rougher, with a large number of obvious spot-like attachments (Fig. 2e), which was consistent with the results of XPS. In general, the increase of surface roughness will enhance the mechanical interlocking and lead to stronger interfacial bonding strength [34] between ACFs and matrix. In our case, the improvement of fiber surface roughness is also beneficial to the interface compatibility between ACFs and APFs, leading to an enhancement in mechanical properties of the papery materials.

3.2. ANFs-reinforced aramid paper

Being modified by the coupling agent, the dispersibility of the aramid fiber has been improved. However, the formation of aramid paper is still poor compared with that from plant fibers caused by the large aspect ratio and low surface activity of the aramid fiber. It is well known that the hydrogen bonds between fibers is the reason why the paper can retain some physical strength [35]. Although aramid fibers had undergone surface modification, there were still few hydrogen bonds that can be formed between fibers. The strength of our original aramid paper was still very low. As already mentioned in the introduction part, we can reinforce the weaker part of the paper by using reinforcing materials when it is impossible to greatly improve the uniformity of the paper and the binding force between the fibers. Taking into account the excellent performance of ANFs and their compatibility with aramid fibers, it is reasonable to use ANFs as aramid paper reinforcing material.

As shown in Fig. 1b, the orange-red solution of the ANFs was obtained by adding the aramid original fibers into a solvent system containing DMSO and KOH. Hydrogen atoms from the amide groups were removed to reduce sharply the hydrogen bonding interactions in the polymer chains, and form the negatively charged nitrogen ion, which increased the electrostatic repulsion between the polymer chains and finally facilitated the formation of ANFs (Fig. 1d). The morphology of ANFs was characterized by AFM (Fig. 4a) and TEM (Fig. 4b). The obtained ANFs have a wide range from 30 ~ 70 nm and lengths about several micrometers.

The schematic illustration of the original aramid paper reinforcement process is shown in Fig. 1c. We deposited a layer of ANFs on both sides of the paper by a simple vacuum filtration process. The

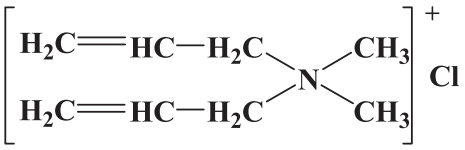

Fig. 3. Chemical Structure of DMDAAC.

distribution of ANFs in the paper structure is shown in Fig. 6e. The deposition of ANFs into the two sides of the whole structure results in the gradient structure, which brings the significant improvement of the strength. As we can know, the surficial strength plays the important role in indicating the whole strength because destroy usually starts from the surficial part of the composites. Hence, this work tries to strengthen the surficial structure by introducing the gradient structures in which deposition of the ANFs produces the stiff structure with decrease progressively across the half thickness direction.

We found that the fibers are rapidly deposited to form a filter cake at the beginning of the vacuum filtration process. As the process goes on, DMSO is hard to pass through the filter cake and the deposited rate becomes slower due to the tiny pore of the filter cake, resulting in a low production efficiency. Therefore, we added a certain amount of flocculant diallyldimethylammonium chloride (DMDAAC) to the ANFs dispersion to accelerate the speed of filtration. DMDAAC is a water-soluble cationic compound with a high positive charge density (Fig. 3) [36]. With the addition of the DMDAAC solution, the color of the nano-aramid dispersion gradually faded to form a stable and transparent solution. The Tyndall effect [37] was observed in both ANFs suspension and flocculated ANFs suspension resulting from the stable colloidal dispersion (Fig. 4d). According to the classical DLVO theory [31], there is not only the repulsive energy between colloids but also the suction potential energy. The former is the electrostatic repulsive force generated by the overlap of the diffusion layers when the charged colloids are close together. The suction potential is the long-range van der Waals force. Schematic diagram of mechanisms for ANFs flocculation was shown in Fig. 4e. Due to the presence of many negative charges in the long-chain of ANFs, DMDAAC molecules would be immediately adsorbed on the ANFs by electrostatic attraction when adding into the ANFs dispersion, leading to the formation of ANFs-DMDAAC composite structure (ADCS). On one hand, ADCS can be close to each other in a certain agglomeration between the nano-aramid fibers because of the long-range van der Waals attraction between adjacent ADCS. On the other hand, a large amount of positive charges distributed on the surface causes a repulsive effect between ADCS. The combination of the forces above renders the overall system finally being in a stable state. Compared with the original ANFs (Fig. 4b), the flocculation nano-aramid fibers are obviously intertwined and look like some black spots (Fig. 4c). By the flocculation of ANFs, the suction filtration time is greatly reduced from 20 h and 30 min to 1 h and 10 min, which greatly improves the preparation efficiency (Fig. 4f). It is worth mentioning that the flocculation of ANFs is only owing to electrostatic and long-range van der Waals forces rather than chemical bonding. Therefore, the ANFs after flocculation still maintain good nano-characteristics so that there is no significant change in the strength after film formation.

3.3. High performance of aramid paper composite

The ANFs-reinforced paper exhibited a yellower color than the original aramid paper (Fig. 5a). The differences from the ideal structure of original aramid paper to the ANFs-reinforced samples were distinctly observed from SEM images by scanning cross-sections and fracture surface. The original aramid paper was loosely composed of large pores, ACFs, and APFs (Fig. 5d). The weak combination and relatively poor dispersion of ACFs and APFs result in rough paper surface and loose paper structure. There is an obvious contrast between the reinforced part and unenhanced part of the paper, which distinctly shows the

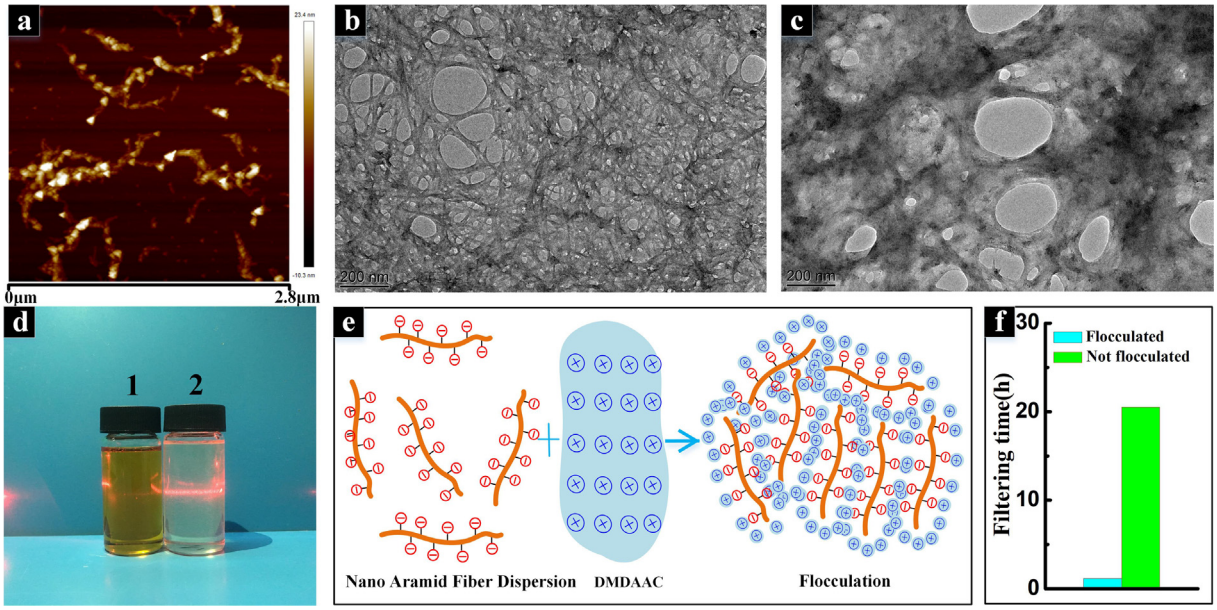

Fig. 4. AFM images (a) and TEM images (b) of ANFs in DMSO solution. (c) TEM images of the flocculated ANFs. (d) Digital photo of ANFs dispersions before (1) and after (2) flocculation. (e) The schematic illustration of the flocculation principle of ANFs. (f) The filtering time of ANFs dispersions. (For interpretation of the references to colour in this figure legend, the reader is referred to the web version of this article.)

strengthening effect of ANFs on paper (Fig. 5b). The flat smooth surface of the ANFs-reinforced paper indicated that the aramid nanofiber with small size and the perfect coverage for paper weaknesses (Fig. 5c). In addition, the ACFs and the ANFs are well combined with each other. The ANFs in small size filled out the pores between the aramid fibers (ACFs and APFs) and glued on the skeleton of the ACFs made the aramid paper more compact. From a partial enlargement (Fig. 5e), we can observe the nano-shape character of ANFs. The cross-sectional SEM photographs of the original aramid paper and the ANFs-reinforced paper treated with the same hot-pressing process are respectively shown in Fig. 5f and g. Compared with the original aramid paper, the reinforced paper has a flatter surface, thinner thickness and more compact paper structure. In fact, the thickness of the original aramid paper is about 230 ± 20 μm, the thickness of the aramid paper after hot-pressing is about 170 ± 20 μm, and the thickness of the ANFs-reinforced paper is further reduced to approximately 130 ± 15 μm. It is undoubtedly that this will contribute to the increase in the physical strength of the paper. One reason for reinforcement is the bridging effect of gradient distributed ANFs, making the ACFs and APFs bond closer together in the paper structure (Fig. 6e). Another one is that there are some DMSO/KOH in the paper structure that has not been completely washed, which will have a definite activation effect, exposing more hydroxyl groups on APFs when performing high-temperature and high-pressure hot pressing.

Fig. 6 shows the morphologies of the uncomplete broken ANFs-reinforced paper crack section (Fig. 6a) and its completely broken cross section (Fig. 6b) and the complete broken cross section of the original aramid paper (Fig. 6c). It can be speculated that the nanometer aramid layer on the surface of the paper first breaks during the tensile strength test, and then the internal structure of the paper is pulled off. It indicates that the increase in paper strength is due primarily to the coating of ANFs. Fig. 6e shows the Interlayer bonding strength (ILSS) test results of the three papers. For the hot-pressed paper, the paper was longitudinally torn apart from the middle after the interlayer bonding strength test, and the average ILSS was 57.265 J/m^2. For the ANFs-reinforced paper, the ANFs layer on the surface was torn apart after the interlayer bond strength test. The average ILSS between the ANFs layer and the core layer was 51.621 J/m^2, which was only slightly smaller than the ILSS of the core layer paper (hot-pressed paper). It can be clearly seen from the SEM photograph that although the ANFs layer is torn apart (Fig. 6d), a large amount of ACFs and APFs adhere to this thin film, which shows that the interlayer bonding force between the ANFs layer and the core layer is sufficient to ensure the overall strength of the paper. Fig. 6e and Fig. 6f show the tensile strength test results for the three papers. The average tensile strength of original paper and hot-pressed paper were 1.16 MPa and 5.65 MPa, respectively. The average tensile strength of ANFs-reinforced paper was 43.7 MPa, which was significantly increased by 36.7 times and 6.7 times compared with original paper and hot-pressed paper, respectively. We also compare the specific strength of papers before and after reinforcement (Fig. 6g). The average specific strength of ANFs-reinforced paper, hot-pressed paper, and original paper are 54576 m^2/s^2, 13050 m^2/s^2, 3622 m^2/s^2, respectively. The specific strength of ANFs-reinforced paper increased by 14.1 times compared with the original paper, which is more favorable for its potential application as a lightweight high-strength material. A comparison of the fracture energy of the papers mentioned above is shown on the left of Fig. 6e. It is worth noting that the fracture energy of the ANFs-reinforced paper has sharply increased by 78 times from 155 J/m^2 to 12241 J/m^2. Compared with other people's work [38–44], this work is of great success in enhancing the strength of aramid paper (Fig. 6f).

Fig. 7 shows the thermogravimetric analysis (TGA) curves of ANFs and aramid paper. On the whole, the ACFs, ANFs, and ANFs-reinforced aramid paper are relatively stable under high-temperature condition with similar thermal stability. The reason why ANFs-reinforced aramid paper has a high weight loss rate before 500 °C is due to the addition of some paper additives such as dispersant PEO, cationic starch, etc. In addition, some moisture and DMSO remain in the paper will decompose and volatilize at lower temperatures. The thermal decomposition residual rate of ACFs is lower than that of ANFs. It is caused by some organic solvents on the surface of ACFs residual in industrial production, while the ANFs do not contain these substances.

4. Conclusions

In summary, the significant enhancement of ANFs to ordinary aramid paper has been demonstrated, and a high-performance nano-aramid composite with a gradient structure can be prepared only by a

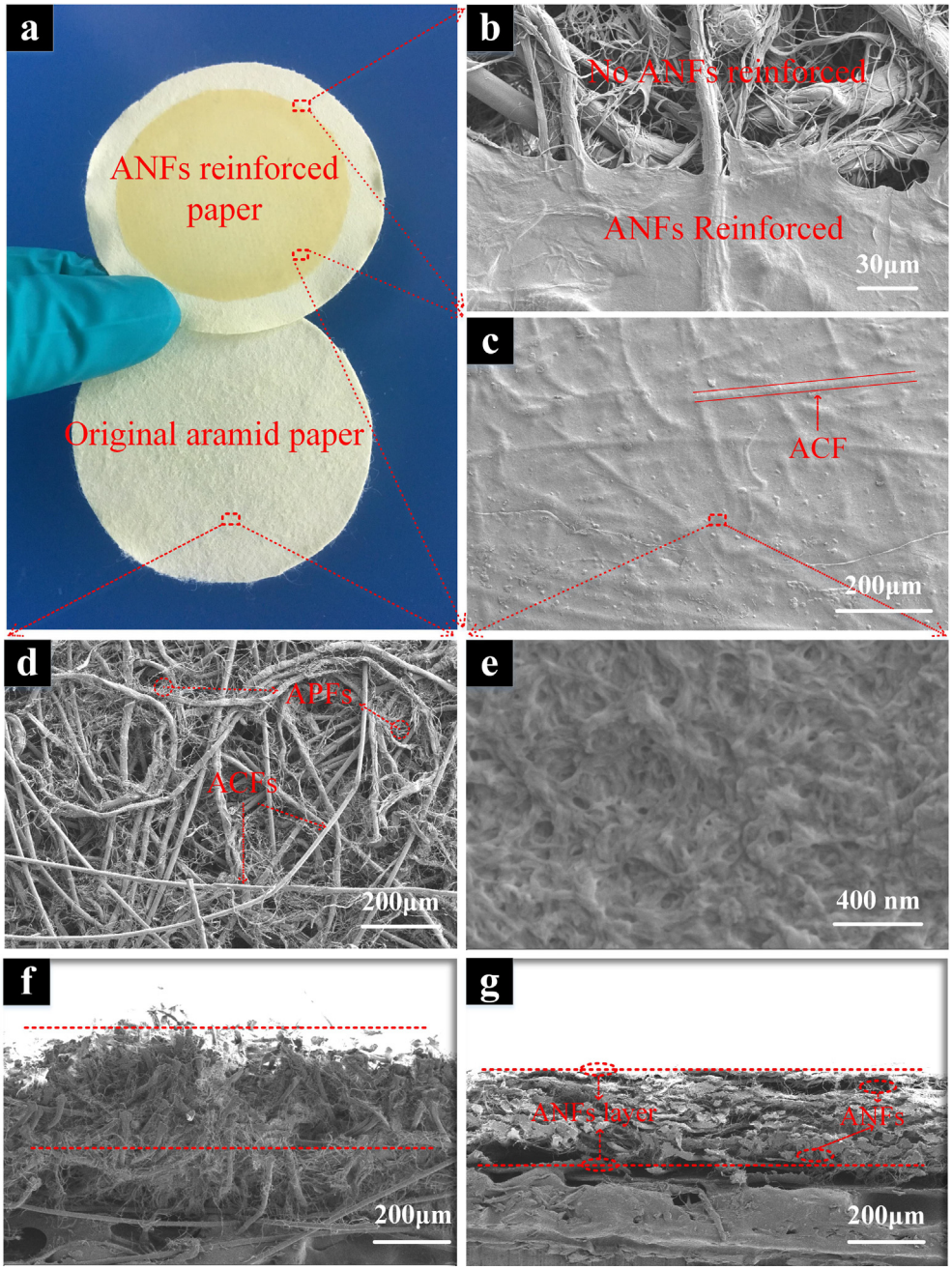

Fig. 5. Digital photo of nano aramid reinforced paper and original aramid paper (a), SEM images of aramid paper surface: (d) original paper, (b), (c), (e) nano aramid reinforced paper; SEM micrographs of the fracture surface: (f) original paper, (g) nano aramid reinforced paper. (For interpretation of the references to colour in this figure legend, the reader is referred to the web version of this article.)

simple vacuum filtration process. ANFs have prominent effects on paper structure, like reinforcement, filling, bridging, etc. In addition, the coupling agent KH-792 improved the inert surface modification of ACFS remarkably. The addition of DMDAAC solution could promote the formation of ANFs on paper and increases the efficiency of the whole process. The reinforced aramid paper has excellent thermal and mechanical properties, and compared to the original aramid paper, its tensile strength, specific strength, and fracture energy are raised 36.7 times, 14.1 times, and 78.0 times, respectively. This work is expected to helpful for the development of lightweight and high-strength honeycomb materials for aircraft fuselages, ships, high-speed trains, and car bodies, as well as insulation materials under high-temperature conditions. And this work also demonstrates the enormous potential of ANFs as a new reinforcement for aramid paper and other high-performance materials.

Acknowledgments

This work was financially supported by the Guangzhou Science and Technology Plan Project (Grant No. 201704030066), Guangdong Province Youth Science and Technology Innovation Talents (Grant No. 2014TQ01C781), Science and Technology Planning Project of Guangdong Province, China (Grant No. 2016B090918074), and the Fundamental Research Funds for the Central Universities, South China University of Technology (Grant No. 2017ZD087). Guangdong Province Science Foundation for Cultivating National Engineering Research Center for Efficient Utilization of Plant Fibers (2017B090903003).

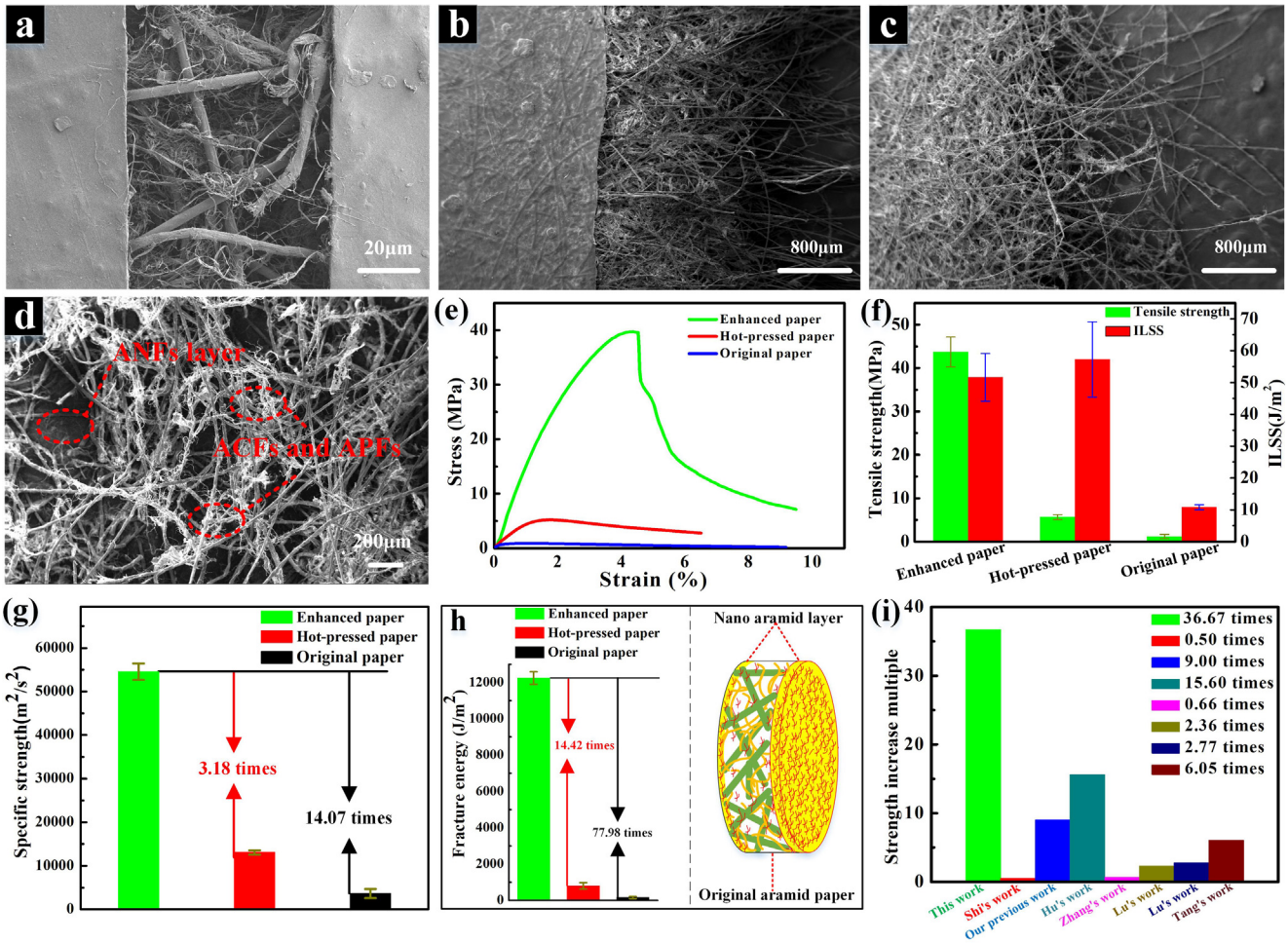

Fig. 6. The fracture surface of the aramid paper, (a) and (b) with ANFs enhancement, (c) without ANFs enhancement. The ANFs layer that was torn apart after the interlayer bond strength test (d). The stress-strain curve of aramid paper (e) and the average tensile strength and ILSS for aramid paper (f). The comparison of specific strength of three kinds of aramid paper (g). the fracture energy changes of aramid paper and the schematic illustration of paper structure (h), the strength increase multiple of ANFs-reinforced paper compared to original paper and comparison with other people's work (i). (For interpretation of the references to colour in this figure legend, the reader is referred to the web version of this article.)

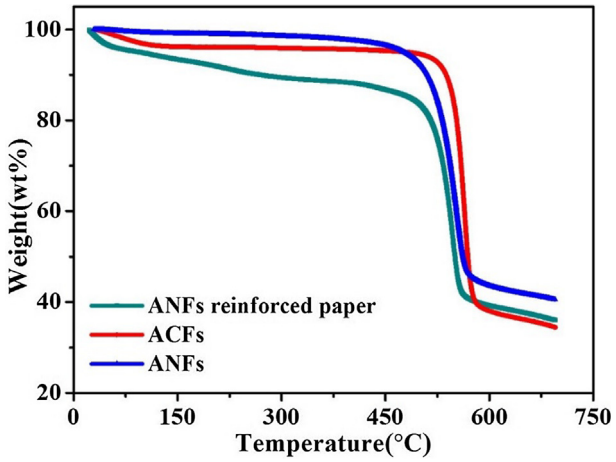

Fig. 7. TGA curves of ANFs, ACFs, and ANFs-reinforced paper. (For interpretation of the references to colour in this figure legend, the reader is referred to the web version of this article.)

References

[1] Goulouti K, Castro JD, Keller T. Aramid/glass fiber-reinforced thermal break – structural system performance. Compos Struct 2016;152:455–63.

[2] Cheng Z, Zhang L, Jiang C, Dai Y, Meng C, Luo L, et al. Aramid fiber with excellent interfacial properties suitable for resin composite in a wide polarity range. Chem Eng J 2018;347:483–92.

[3] Cao K, Siepermann CP, Yang M, Waas AM, Kotov NA, Thouless MD, et al. Reactive aramid nanostructures as high-performance polymeric building blocks for advanced composites. Adv Funct Mater 2013;23(16):2072–80.

[4] Cheng Z, Hong D, Dai Y, Jiang C, Meng C, Luo L, et al. Highly improved Uv resistance and composite interfacial properties of aramid fiber via iron (III) coordination. Appl Surf Sci 2018;434:473–80.

[5] Zhao Y, Dang W, Lu Z, Deng J, Hao Y, Su Z, et al. Fabrication of mechanically robust and UV-resistant aramid fiber-based composite paper by adding nano-TiO_2 and nanofibrillated cellulose. Cellulose 2018;25(7):3913–25.

[6] Nyholm L, Nyström G, Mihranyan A, Strømme M. Toward flexible polymer and paper-based energy storage devices. Adv Mater 2011;23(33):3751–69.

[7] Liao X, Zhang Z, Liao Q, Liang Q, Ou Y, Xu M, et al. Flexible and printable paper-based strain sensors for wearable and large-area green electronics. Nanoscale 2016;8(26):13025.

[8] Russo A, Ahn BY, Adams JJ, Duoss EB, Bernhard JT, Lewis JA. Pen-on-paper flexible electronics. Adv Mater 2011;23(30):3426–30.

[9] Daniel T, Ronald O. Sterbacka Paper Electronics. Adv Materials. 2011;23(17):1935–61.

[10] Tai YL, Yang ZG. Fabrication of paper-based conductive patterns for flexible electronics by direct-writing. J Mater Chem 2011;21(16):5938–43.

[11] García JM, García FC, Serna F, Peña JLDL. High-performance aromatic polyamides. Prog Polym Sci 2010;35(5):623–86.

[12] Sa R, Yan Y, Wei Z, Zhang L, Wang W, Tian M. Surface modification of aramid fibers by bio-inspired poly(dopamine) and epoxy functionalized silane grafting. Acs Appl Mater Interf 2014;6(23):21730–8.

[13] Kong H, Teng C, Liu X, Zhou J, Zhong H, Zhang Y, et al. Simultaneously improving the tensile strength and modulus of aramid fiber by enhancing amorphous phase in supercritical carbon dioxide. RSC Adv 2014;4(39):20599–604.

[14] Cheng Z, Li B, Huang J, Chen T, Liu Y, Wang X, et al. Covalent modification of

Aramid fibers' surface via direct fluorination to enhance composite interfacial properties. Mater Des 2016;106:216–25.
[15] Cheng Z, Jiang C, Dai Y, Meng C, Luo L, Liu X. Fe3 + coordination induced selective fluorination of aramid fiber to suppress surface chain scission behavior and improve surface polarity. Appl Surf Sci 2018;456:221–9.
[16] Chen J, Zhu Y, Ni Q, Fu Y, Fu X. Surface modification and characterization of aramid fibers with hybrid coating. Appl Surf Sci 2014;321(321):103–8.
[17] Wang L, Shi Y, Sa R, Ning N, Wang W, Tian M, et al. Modification of Aramid fibers by catechol/polyamine co-deposition followed silane grafting for the enhanced interfacial adhesion to rubber. Matrix Industrial Eng Chem Res 2016;55(49).
[18] Yuan H, Wang W, Yang D, Zhou X, Zhao Z, Zhang L, et al. Hydrophilicity modification of aramid fiber using a linear shape plasma excited by nanosecond pulse. Surf Coat Technol 2018;344:614–20.
[19] Wang J, Chen P, Lu C, Yu Q, Li W, Ren R. Improvement of aramid fiber III reinforced bismaleimide composite interfacial adhesion by oxygen plasma treatment. Compos Interf 2018;2:1–13.
[20] Sun Y, Liang Q, Chi H, Zhang Y, Shi Y, Fang D, et al. The application of gas plasma technologies in surface modification of aramid fiber. Fibers Polym 2014;15(1):1–7.
[21] Wang CX, Du M, Lv JC, Zhou QQ, Ren Y, Liu GL, et al. Surface modification of aramid fiber by plasma induced vapor phase graft polymerization of acrylic acid. I. Influence of plasma conditions. Appl Surf Sci 2015;349:333–42.
[22] Xing L, Liu L, Huang Y, Jiang D, Jiang B, He J. Enhanced interfacial properties of domestic aramid fiber-12 via high energy gamma ray irradiation. Compos B Eng 2015;69:50–7.
[23] Liu L, Huang YD, Zhang ZQ, Jiang ZX, Wu LN. Ultrasonic treatment of aramid fiber surface and its effect on the interface of aramid/epoxy composites. Appl Surf Sci 2008;254(9):2594–9.
[24] Wang L, Shi Y, Chen S, Wang W, Tian M, Ning N, et al. Highly efficient mussel-like inspired modification of aramid fibers by UV-accelerated catechol/polyamine deposition followed chemical grafting for high-performance polymer composites. Chem Eng J 2017;314:583–93.
[25] Broek D. Elementary engineering fracture mechanics. J Appl Mech 1986;42(3):751–2.
[26] Yang M, Cao K, Sui L, Qi Y, Zhu J, Waas A, et al. Dispersions of aramid nanofibers: a new nanoscale building block. Acs Nano 2011;5(9):6945.
[27] Guan Y, Li W, Zhang Y, Shi Z, Tan J, Wang F, et al. Aramid nanofibers and poly (vinyl alcohol) nanocomposites for ideal combination of strength and toughness via hydrogen bonding interactions. Compos Sci Technol 2017;144:193–201.
[28] Lin J, Sun HB, Malakooti MH, Sodano HA. Isolation of Aramid nanofibers for high strength and toughness polymer nanocomposites. Acs Appl Mater Interf 2017;9(12):11167–75.
[29] Zhu J, Cao W, Yue M, Hou Y, Han J, Yang M. Strong and stiff aramid nanofiber/carbon nanotube nanocomposites. Acs Nano 2015;9(3):2489–501.
[30] Kwon SR, Harris J, Zhou T, Loufakis D, Boyd JG, Lutkenhaus JL. Mechanically strong graphene/aramid nanofiber composite electrodes for structural energy and power. Acs Nano 2017;11(7).
[31] Hiemenz PC. Principles of Colloid Surface Chemistry 1977.
[32] Liu L, Huang YD, Zhang ZQ, Jiang B, Nie J. Ultrasonic modification of aramid fiber–epoxy interface. J Appl Polym Sci 2010;81(11):2764–8.
[33] Liu L, Zhang X, Huang Y, Jiang B, Zhiqian Z. Effect of ultrasonic treatment on surface characteristics of Aramid. Acta Materiae Compositae Sinica 2003;20(2):35–40.
[34] Yuan G, Bai Y, Jia Z, Hui D, Lau KT. Enhancement of interfacial bonding strength of SMA smart composites by using mechanical indented method. Compos B 2016;106:99–106.
[35] Neimo L. Papermaking Chem. 1999.
[36] Wandrey C, Hernández-Barajas J, Hunkeler D. Diallyldimethylammonium chloride and its polymers. Heidelberg: Springer, Berlin; 1999.
[37] Laser Thomas E. Pointer and the Tyndall effect. J Chem Educ 1996;73(73):;págs:470-.
[38] Shi Y, Wang B. Mechanical properties of carbon fiber/cellulose composite papers modified by hot-melting fibers. Progress Natural Sci: Mater Int 2014;24(1):56–60.
[39] Ou Y, Chen J, Lu P, Cheng F, Lin M, Su L, et al. Rapid ILs-polishing processes toward flexible nanostructured paper with dually high transparency and haze. Sci Rep 2017;7(1).
[40] Hu W, Chen G, Liu Y, Liu Y, Li B, Fang Z. Transparent and hazy all-cellulose composite films with superior mechanical properties. Acs Sustain Chem Eng 2018.
[41] Zhang SF, Zhang MJ, Dou WW, Peng-Hui LI, Yuan L, Dan L. Effects of modified Nano-SiO_2 fillers on mechanical properties of aramid paper. China Pulp Paper 2015.
[42] Lu Z, Hu W, Xie F, Hao Y. Highly improved mechanical strength of aramid paper composite via a bridge of cellulose nanofiber. Cellulose 2017;24(7):2827–35.
[43] Tang AM, Li DG, Zhao S, Jia CF. The reinforce effect of polyimide resin on PPTA paper. China Pulp Paper 2015.
[44] Lu Z, Dang W, Zhao Y, Wang L, Zhang M, Liu G. Toward high-performance poly (para-phenylene terephthalamide) (PPTA)-based composite paper via hot-pressing: the key role of partial fibrillation and surface activation. RSC Adv 2017;7(12):7293–302.